New Journal of Physics
The open-access journal for physics

Relativistic plasma surfaces as an efficient second harmonic generator

M J V Streeter[1,2,8], P S Foster[1,3], F H Cameron[1], M Borghesi[3], C Brenner[1,4], D C Carroll[4], E Divall[1], N P Dover[2], B Dromey[3], P Gallegos[1,4], J S Green[1], S Hawkes[1], C J Hooker[1], S Kar[3], P McKenna[4], S R Nagel[2], Z Najmudin[2], C A J Palmer[2], R Prasad[3], K E Quinn[3], P P Rajeev[1], A P L Robinson[1], L Romagnani[3,5], J Schreiber[2,6,7], C Spindloe[1], S Ter-Avetisyan[3], O Tresca[4], M Zepf[3] and D Neely[1,4]

[1] Central Laser Facility, STFC, Rutherford Appleton Laboratory, Didcot OX11 0QX, UK
[2] Blackett Laboratory, Imperial College London, London SW7 2AZ, UK
[3] School of Mathematics and Physics, Queen's University Belfast, Belfast BT7 1NN, UK
[4] Department of Physics, SUPA, University of Strathclyde, Glasgow G4 0NG, UK
[5] LULI, École Polytechnique, CNRS, CEA, UPMC, route de Saclay, 91128 Palaiseau, France
[6] Max-Planck-Institut für Quantenoptik, Garching, Germany
[7] Department für Physik, Ludwig-Maximilians-Universität München, Garching, Germany
E-mail: m.streeter09@imperial.ac.uk

New Journal of Physics **13** (2011) 023041 (10pp)
Received 17 November 2010
Published 24 February 2011
Online at http://www.njp.org/
doi:10.1088/1367-2630/13/2/023041

Abstract. We report on the characterization of the specular reflection of 50 fs laser pulses in the intensity range 10^{17}–10^{21} W cm^{-2} obliquely incident with p-polarization onto solid density plasmas. These measurements show that the absorbed energy fraction remains approximately constant and that second harmonic generation (SHG) achieves efficiencies of $22 \pm 8\%$ for intensities approaching 10^{21} W cm^{-2}. A simple model based on the relativistic oscillating mirror concept reproduces the observed intensity scaling, indicating that this is

[8] Author to whom any correspondence should be addressed.

the dominant process involved for these conditions. This method may prove to be superior to SHG by sum frequency mixing in crystals as it is free from dispersion and retains high spatial coherence at high intensity.

Contents

1. Introduction

With increasing laser intensity and decreasing pulse duration, plasma-based optics become a more attractive way of temporally and spatially manipulating ultrashort laser pulses [1]. They can also be used to generate harmonics of the laser frequency as the result of two main processes, which are described by the coherent wakefield emission (CWE) [2] and the relativistically oscillating mirror [3, 4] (ROM) models. For the case of p-polarized interactions these processes are both capable of generating second harmonic emission in the specular direction with conversion efficiencies predicted to be in excess of 40% [5]. The conventional method for second harmonic generation (SHG) for laser applications is frequency doubling through nonlinear interactions in birefringent crystals, such as potassium dihydrogen phosphate (KDP), which achieves similar efficiencies for femtosecond laser pulses. However, this also produces adverse effects, such as pulse stretching by group velocity dispersion, self-phase modulation and self-focusing [6, 7], which can reduce the spatial coherence of the beam. These nonlinear effects are considered to have an appreciable detrimental effect when the B-integral exceeds unity, where $B = 2\pi\lambda_0^{-1}\int n_2 I(z)\,\mathrm{d}z$ for laser wavelength λ, intensity I and propagation axis z, and where n_2 is the Kerr nonlinearity of the medium. In the case of a 15 J 50 fs laser[9] with a beam diameter of 15 cm, using a 300 μm KDP crystal would introduce a B-integral of $\sim$10, which would limit the subsequent maximum achievable intensity [8]. By contrast, harmonics produced from the surface of solid target interactions do not stretch the pulse [9] and exhibit very high spatial coherence as long as the target remains flat throughout the interaction [10, 11].

CWE occurs as electron bunches, pulled out of the plasma by the component of the electric field that is parallel to the density gradient [12], are accelerated up the plasma density gradient generating plasma oscillations in their wake. As the electrons are temporally bunched at intervals of the laser period, plasma frequencies that are integer multiples of the laser frequency are resonantly excited, generating harmonics up to the plasma frequency corresponding to the maximum density of the target. In the ROM process, the region from which the laser

[9] These are the characteristics of the Astra Gemini laser used in the experiments reported here.

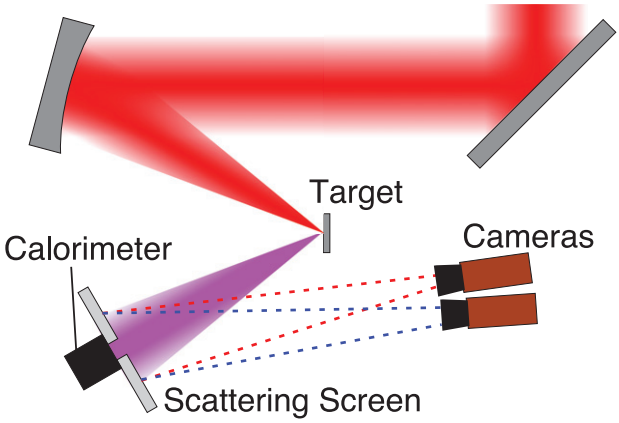

Figure 1. Schematic diagram of the experimental setup showing the focusing geometry and the specular reflectivity monitor.

of frequency ω_0 is reflected, given by the critical density $n_{\mathrm{crit}} = \omega_0^2 m_e \epsilon_0 / e^2$, is considered to oscillate in the laser field. Since the reflection point moves during the period of the driving pulse, the phase of the reflected wave is redistributed. In particular, as the critical density surface moves towards the laser, it compresses the pulse, creating rapid changes in phase, resulting in the generation of high harmonics. The motion of the surface is a function of the intensity, angle of incidence and polarization, as well as the local density gradient, which dictates the restoring force of the plasma opposing the displacement due to the laser field.

These mechanisms are differentiated by their intensity dependence [13] and the phase of the resultant harmonics [9]. There is also a maximum harmonic cutoff for CWE corresponding to the maximum plasma density [2], whereas the maximum ROM harmonic number is dictated by γ_{max}, the maximum relativistic gamma factor of the critical surface motion [14].

The plasma scale length, defined as $L = n_e(\mathrm{d}n_e/\mathrm{d}x)^{-1}$ at the critical density surface, where n_e is the electron density, has an important role in determining the efficiencies of both methods of harmonic production [15, 16]. This is difficult to measure directly during experiment, but the variation of scale length with intensity can be qualitatively determined by monitoring the specularly reflected laser energy [17].

2. Experimental setup

The experiment was carried out using the Astra Gemini laser [18], which delivered 12 J in a 50 fs pulse at the central wavelength $\lambda_0 = 800$ nm. Figure 1 shows the setup in which an $f/2$ parabola focused the laser onto targets at 35° angle of incidence with p-polarization to create a focal spot with 2.5 μm full-width at half-maximum (FWHM) containing ~35% of the laser energy. The contrast, defined as the ratio of the intensity of the preceding amplified spontaneous emission (ASE) to the peak intensity, was measured using a scanning autocorrelator as 10^{-6}. Double plasma mirrors [19] were used to increase this to 10^{-10}. The intensity on the target was varied in the range of 10^{17}–10^{21} W cm^{-2} by defocusing the focal spot by moving the focusing parabola relative to the target, hence keeping the energy on the target constant. The targets were 0.1 μm optically flat [20] aluminium foils.

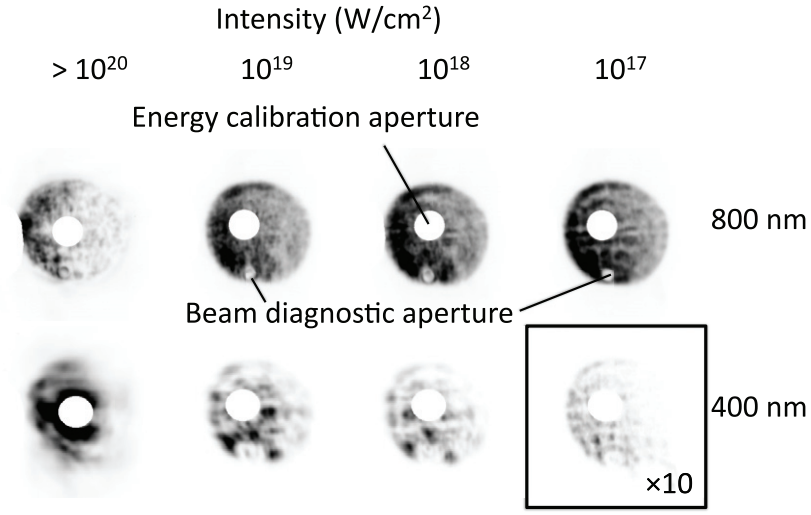

Figure 2. Images of the specularly reflected beam. The top line shows the 800 nm (ω_0) and the second line the 400 nm ($2\omega_0$) images from the same shots. The small hole at the bottom of the beam, visible in the ω_0 image, is caused by a hole in a mirror at the output of the compressor used for pulse length measurement. The central hole was used to calibrate the camera for energy measurements. Note that the brightness of the $2\omega_0$ image for 10^{17} W cm^{-2} has been multiplied by a factor of 10 to make it visible on the same scale.

The specularly reflected light from the target was incident on a plastic scattering screen, which was imaged by two cameras, each with an interference filter, one centred at 800 nm with 25 nm bandwidth, corresponding to the fundamental frequency ω_0, and the other centred at 400 nm with 10 nm bandwidth to observe the second harmonic $2\omega_0$. The screen covered an angular range equivalent to an $f/0.62$ cone and had a 31 mm diameter circular aperture cut in the centre to allow direct energy calibration with a surface absorbing calorimeter. Several low-intensity shots were taken to ensure that almost all the energy incident on the energy meter was at ω_0 with a relatively uniform intensity profile, providing a calibration of the camera signal with the calorimeter. The 400 nm camera was calibrated relative to the 800 nm camera by taking into account the relative responses of the cameras and the opacity of their respective filters at the relevant wavelength. The reflected energy for each wavelength was measured by integrating the signal on the scattering screen, compensating for the holes and edges of the screen. This adjustment was typically ~10% of the total energy.

3. Experimental results

Figure 2 shows sample images observed during the intensity scan. No qualitative difference in the 800 nm images was seen until the intensity became $I > 10^{20}$ W cm^{-2}, at which point the signal became noticeably weaker. However, even at the highest intensities the beam profile remained constant in size, although with increasingly fine (higher spatial frequency) modulations. This indicates that the plasma surface remained relatively flat over the timescale of the interaction for all the shots. The $2\omega_0$ image was very weak by comparison for $I = 10^{17}$ W cm^{-2}, but became much brighter as the intensity was increased.

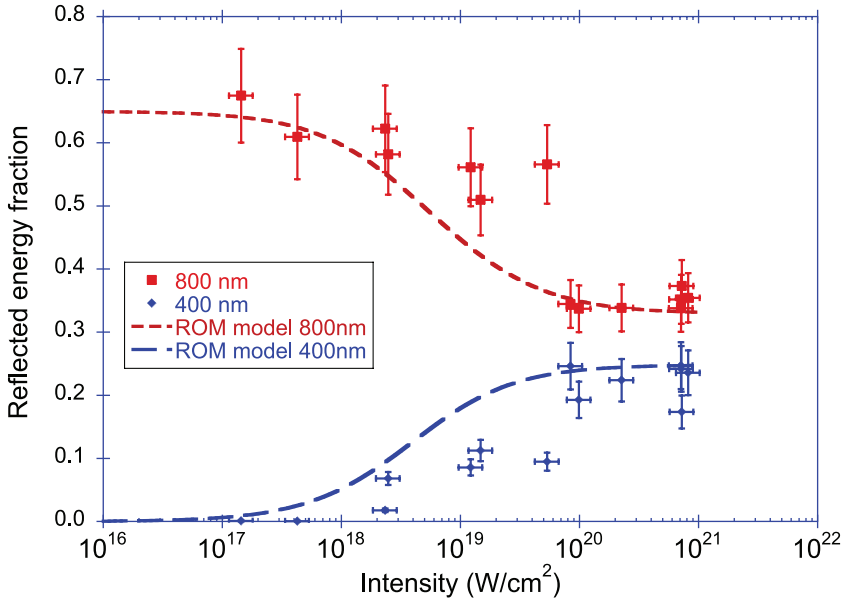

Figure 3. Energy incident onto the scattering screen as observed at 800 nm (squares) and 400 nm (diamonds). Vertical error bars are combined calibration and measurement errors. In the region near the focus, the intensity was calculated as the mean within the FWHM radius; away from the focus, it is the mean intensity within the beam radius. The dashed lines represent the results of the ROM model.

The observed 400 and 800 nm energy on the screen as a fraction of incident laser energy is shown in figure 3. Measurements of the specular 400 nm beam show the conversion efficiency to $2\omega_0$ increasing to $22(\pm 8)\%$ as the intensity rises up to $10^{21}\,\mathrm{W\,cm^{-2}}$ and is consistent with a previous work [21] giving a $>5\%$ efficiency at $10^{19}\,\mathrm{W\,cm^{-2}}$. The energy converted to $2\omega_0$ represents a significant fraction of the incident laser energy and accounts for most of the reduction in reflected 800 nm energy.

The reflected ω_0 beam profile shows a loss of brightness while retaining the same beam structure as the intensity is increased. Higher spatial frequency modulations will be spread over a larger area in the focal plane and thus will be reflected from regions of lower intensity, which retain high reflectivity. The lower spatial frequencies, however, will be concentrated in the high-intensity regions, where they are preferentially attenuated by nonlinear processes such as absorption, scattering, transmission or frequency conversion. This would give rise to the high-frequency modulations seen at the highest intensities and is analogous to spatial filtering with a high-pass filter.

The profile of the second harmonic beam matches the ω_0 beam profile at lower intensities, although for $I > 10^{19}\,\mathrm{W\,cm^{-2}}$ it becomes more centrally peaked. The $2\omega_0$ beam is also noteworthy for the relative absence of high spatial frequencies at all intensities, as compared to the ω_0 profile, but especially for $I > 10^{20}\,\mathrm{W\,cm^{-2}}$. This reiterates that this feature seen in the ω_0 beam is not due to beam break-up, as otherwise this would manifest itself in the $2\omega_0$ profile. At tight focus the $2\omega_0$ production efficiency is more efficient in the centre than in the wings, preferentially filtering out high spatial frequencies of the input beam and resulting in a more Gaussian beam at $2\omega_0$. Hence, in stark contrast to other methods of SHG, this process has the ability to increase the M^2 quality as compared to the input beam.

4. The relativistically oscillating mirror (ROM) model

To calculate the motion of the plasma surface caused by the electromagnetic field of the incident laser, the surface is modelled as an infinite sheet of electrons with an immobile ion background, based on the methods in [4, 22]. All electrons are assumed to move in the same way, which is given by solving the electron motion in a plane parallel wave propagating in vacuum for which the time-averaged electron position remains constant. Given these conditions, the Lorentz force equation is reduced to the following for the relativistic parameter, $\gamma = (1 - (\mathbf{v}/c)^2)^{-1/2}$,

$$\gamma = \frac{a^2 + \alpha^2 + 1}{2\alpha}, \tag{1}$$

and the longitudinal and transverse velocity components

$$v_\perp = \frac{2a\alpha c}{a^2 + \alpha^2 + 1}, \quad v_\parallel = \frac{(a^2 - \alpha^2 + 1)\, c}{a^2 + \alpha^2 + 1}, \tag{2}$$

where a is the normalized vector potential and α is a constant of integration.

For the ROM model any drift velocity will be eliminated as long as the average position of the solid surface is assumed to remain constant. This is done by finding the value of α for which the time-averaged $v_\parallel$ is zero. Equations (2) can then be integrated to give the particle position as a function of time. The projection of this particle motion onto the target normal axis gives the surface motion of the oscillating mirror.

The phase of the reflected beam is redistributed by the motion of the reflecting surface, and as the periodicity of the plasma surface is phase locked to the laser field, this results in harmonics being generated in the reflected pulse.

The reflected pulse at a point is given by

$$E_\mathrm{r} = E_0 \sin(\omega_0 t'), \tag{3}$$

where E_0 is the amplitude of the electric field and

$$t' = t + \frac{2\, z' \cos\theta}{c}. \tag{4}$$

Here, t' and z' are the retarded time and position, respectively, and θ is the angle of incidence. The retarded position is the position of the surface when the laser light that passed a fixed point at time t reflects off it. This position is obtained numerically, which allows the reflected field to be calculated. The plasma surface motion is calculated for the given intensity, whereas the input field is given a $\sin^2(t/T)$-intensity envelope where T is the pulse length, which is set to 50 fs. Figure 4 shows the motion of the ROM and the electric field distribution for intensities ranging from 10^{17} to $10^{20}\,\mathrm{W\,cm^{-2}}$, showing the increasing nonlinearity in the reflected pulse due to the Doppler redistribution of photon energy.

The Fourier transform of the reflected field gives the spectral content and the strengths of ω_0 and $2\omega_0$ are then found as fractions of the total energy in the spectrum. The results of the ROM mode are compared to the experimental results in figure 3. As absorption is not included in the model, all values were multiplied by 0.65 to represent the absorption inferred from the experimental measurements. The model closely follows the measured ω_0 and $2\omega_0$ reflectivities

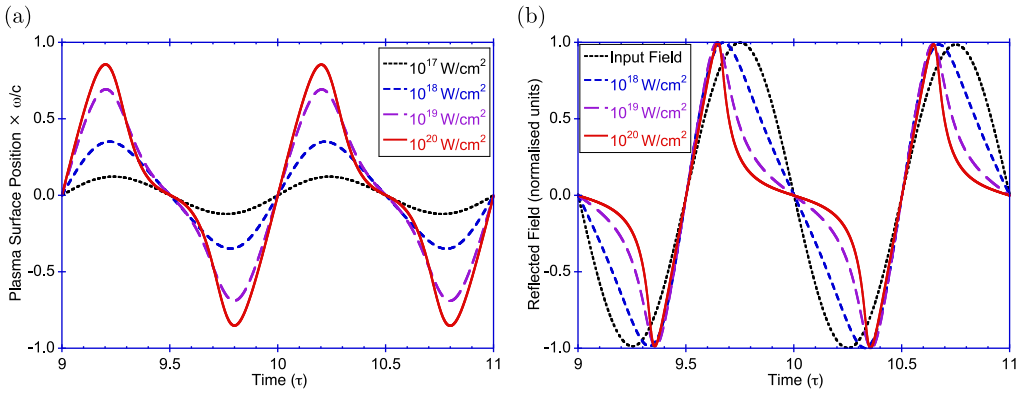

Figure 4. Two cycles of (a) the plasma surface position and (b) the reflected electric fields, normalized to the maximum amplitude at each intensity, given by the ROM model (the deviation from the input field is negligible for 10^{17} W cm^{-2}). τ is the period of the laser.

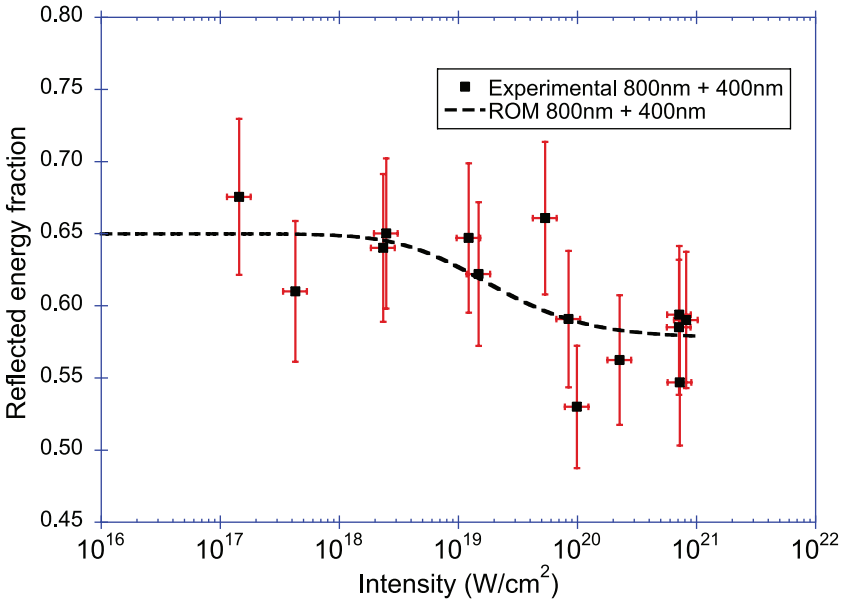

Figure 5. Specular reflectivity into ω_0 and $2\omega_0$ given by the model and measured experimentally. Potential calibration errors are not included in the error bars in order to allow easier relative comparison with the model.

and also displays the saturation in SHG efficiency and ω_0 reflectivity at the level determined experimentally.

The model also predicts that the sum of ω_0 and $2\omega_0$ should decrease as a fraction of the total specularly reflected energy by up to 7% at the highest intensities (see dashed line in figure 5). This is due to the increasing production of higher harmonics. However, the predicted efficiencies of the higher harmonics were not validated in this experiment. The measured value of this combined reflected light at 400 and 800 nm shows an average drop of 8% for $I > 10^{20}$ W cm^{-2}. This indicates that additional energy loss mechanisms, such as absorption or scattering, did not significantly increase in magnitude.

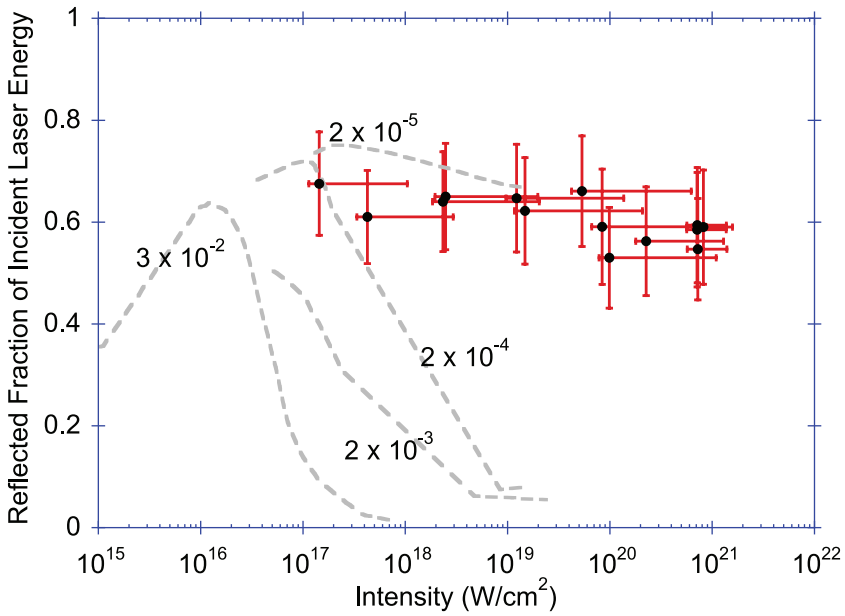

Figure 6. Reflectivity as a function of intensity. Combined ω_0 and $2\omega_0$ signal from this experiment plotted alongside data previously collated in [17]. Note the contrast quoted here is the ratio of energy in the ASE to that in the main pulse (as opposed to intensity contrast as used elsewhere in this paper).

5. Discussion

Both the measurements and the model show that the efficiency of SHG here is intensity dependent and becomes efficient only in the relativistic regime $I\lambda^2 > 10^{18}\,\mathrm{W}\mu\mathrm{m}\,\mathrm{cm}^{-2}$ [15]. The good agreement between the two indicates that the ROM process is dominant. CWE, on the other hand, is only weakly dependent on intensity and is efficient at intensities above $10^{16}\,\mathrm{W}\,\mathrm{cm}^{-2}$ [2], which implies that it is unlikely to be a major contribution to our observed SHG. However, the scale length of the plasma at the time of the interaction, which has a significant effect on the efficiency of harmonics generated by either process [15, 16], was not measured directly.

Figure 6 shows that the *total* specular reflectivity (combined ω_0 and $2\omega_0$) of the plasma was approximately constant over the intensity range 10^{17}–$10^{21}\,\mathrm{W}\,\mathrm{cm}^{-2}$. This puts an upper limit on the plasma absorption which does not significantly change with intensity, unlike previous results [23, 24]. This disagreement may be due to the differing relationship between intensity and plasma scale length for the different experiments. For the high-contrast interactions studied here, the plasma scale length will have remained relatively short over the intensity range. Hence, we did not observe the rapid decrease in reflectivity seen previously above a certain threshold intensity, for lower contrast measurements. This emphasizes the importance of the plasma scale length in determining the absorbed fraction of laser energy in this intensity range [25, 26].

There is a close correlation between the reflectivity for this experiment and for the $E_{\mathrm{ASE}}/E = 2 \times 10^{-5}$ (energy contrast) data set taken with Astra, which has the same front end and first three amplifiers as Gemini. This suggests that the contrast levels were similar for both experiments and is consistent with our measurements and calculations for this experiment, which give $E_{\mathrm{ASE}}/E \approx 2 \times 10^{-5}$ for a nanosecond scale ASE.

6. Conclusions

The conversion efficiency for the generation of second harmonic was observed to be 22(±8)% for intensities greater than $10^{20}\,\mathrm{W\,cm^{-2}}$. This conversion efficiency is comparable to that achievable with an optimized KDP frequency doubling crystal, but without the problems of pulse stretching and reduced spatial coherence, provided the quality of the plasma surface is maintained. Optimizing this process would allow for extremely high-contrast, high-intensity laser–plasma interactions with 400 nm femtosecond pulses.

A model based on the relativistic oscillating mirror concept agrees well with the observed reflectivities. This indicates that this is the dominant mechanism for SHG for the intensity range 10^{17}–$10^{21}\,\mathrm{W\,cm^{-2}}$ for ultrashort pulses with high contrast. The model also suggests that the conversion efficiency into the second harmonic with this process saturates at ∼22% for intensities $>10^{19}\,\mathrm{W\,cm^{-2}}$ at 35° angle of incidence.

In addition, the specular reflectivity of the plasma reveals that plasma absorption remains almost constant over four orders of magnitude in intensity. We attribute this difference to previous measurements to be due to their much lower laser contrast in comparison to the experiment described here. The 8% drop in reflectivity, which is observed for intensities $>10^{19}\,\mathrm{W\,cm^{-2}}$, indicates that extra absorption, scattering or higher harmonic generation processes are occurring in this range.

The high reflectivity at high intensities is obviously advantageous when attempting to optimize the conversion of laser energy into high harmonics. The ROM model suggests that 7% of the reflected energy can be attributed to higher harmonic generation, but the measurement of high harmonics at these high intensities with these high-contrast ultrashort pulses remains to be realized.

Acknowledgments

We are grateful to the Central Laser Facility for excellent support. The experiment was performed as part of the LIBRA Basic Technology consortium (grant no. EP/E035728/1).

References

[1] Gold D M 1994 Direct measurement of prepulse suppression by use of a plasma shutter *Opt. Lett.* **19** 2006–8
[2] Quéré F, Thaury C, Monot P, Dobosz S, Martin P, Geindre J-P and Audebert P 2006 Coherent wake emission of high-order harmonics from overdense plasmas *Phys. Rev. Lett.* **96** 125004
[3] Bulanov S V, Naumova N M and Pegoraro F 1994 Interaction of an ultrashort, relativistically strong laser pulse with an overdense plasma *Phys. Plasmas* **1** 745–57
[4] Lichters R, Meyer ter Vehn J and Pukhov A 1996 Short-pulse laser harmonics from oscillating plasma surfaces driven at relativistic intensity *Phys. Plasmas* **3** 3425–37
[5] Gibbon P 1996 Harmonic generation by femtosecond laser–solid interaction: a coherent 'water-window' light source? *Phys. Rev. Lett.* **76** 50–3
[6] Marcinkevičius A, Tommasini R, Tsakiris G D, Witte K J, Gaižauskas E and Teubner U 2004 Frequency doubling of multi-terawatt femtosecond pulses *Appl. Phys.* B **79** 547–54
[7] Mironov S, Lozhkarev V, Ginzburg V and Khazanov E 2009 High-efficiency second-harmonic generation of superintense ultrashort laser pulses *Appl. Opt.* **48** 2051–7
[8] Neely D *et al* 1999 Frequency doubling of multi-terawatt picosecond pulses *Laser Part. Beams* **17** 281–6

[9] Quéré F, Thaury C, Geindre J-P, Bonnaud G, Monot P and Martin P 2008 Phase properties of laser high-order harmonics generated on plasma mirrors *Phys. Rev. Lett.* **100** 095004
[10] Gordienko S, Pukhov A, Shorokhov O and Baeva T 2005 Coherent focusing of high harmonics: a new way towards the extreme intensities *Phys. Rev. Lett.* **94** 103903
[11] Geissler M, Rykovanov S, Schreiber J, Meyer ter Vehn J and Tsakiris G D 2007 3D simulations of surface harmonic generation with few-cycle laser pulses *New J. Phys.* **9** 218
[12] Brunel F 1987 Not-so-resonant, resonant absorption *Phys. Rev. Lett.* **59** 52–5
[13] Thaury C *et al* 2007 Plasma mirrors for ultrahigh-intensity optics *Nat. Phys.* **3** 424–9
[14] Baeva T, Gordienko S and Pukhov A 2006 Theory of high-order harmonic generation in relativistic laser interaction with overdense plasma *Phys. Rev.* E **74** 046404
[15] Tarasevitch A, Lobov K, Wünsche C and von der Linde D 2007 Transition to the relativistic regime in high order harmonic generation *Phys. Rev. Lett.* **98** 103902
[16] Geindre J P, Marjoribanks R S and Audebert P 2010 Electron vacuum acceleration in a regime beyond brunel absorption *Phys. Rev. Lett.* **104** 135001
[17] Pirozhkov A S *et al* 2009 Diagnostic of laser contrast using target reflectivity *Appl. Phys. Lett.* **94** 241102
[18] Hooker C J *et al* 2006 The Astra Gemini project: a dual-beam petawatt Ti : sapphire laser system *J. Physique* IV **133** 673–7
[19] Ziener C, Foster P S, Divall E J, Hooker C J, Hutchinson M H R, Langley A J and Neely D 2003 Specular reflectivity of plasma mirrors as a function of intensity, pulse duration and angle of incidence *J. Appl. Phys.* **93** 768–70
[20] Spindloe C and Lowe H F 2006–7 White light interferometric profiling of ultra-thin foil high power laser targets *CLF Annu. Rep.* 247
[21] Horlein R *et al* 2008 High contrast plasma mirror: spatial filtering and second harmonic generation at 10^{19} W cm^{-2} *New J. Phys.* **10** 083002
[22] Landau L D and Lifshitz E M 1975 *The Classical Theory of Fields* (Oxford: Pergamon) pp 112–3
[23] Ping Y *et al* 2008 Absorption of short laser pulses on solid targets in the ultrarelativistic regime *Phys. Rev. Lett.* **100** 085004
[24] Davies J R 2009 Laser absorption by overdense plasmas in the relativistic regime *Plasma Phys. Control. Fusion* **51** 014006
[25] Haines M, Wei M, Beg F and Stephens R 2009 Hot-electron temperature and laser-light absorption in fast ignition *Phys. Rev. Lett.* **102** 1–4
[26] Kemp A, Sentoku Y and Tabak M 2008 Hot-electron energy coupling in ultraintense laser–matter interaction *Phys. Rev. Lett.* **101** 8–11